© 2019. Published by The Company of Biologists Ltd | Development (2019) 146, dev175430. doi:10.1242/dev.175430

STEM CELLS AND REGENERATION

RESEARCH REPORT

BMP4 patterns Smad activity and generates stereotyped cell fate organization in spinal organoids

Nathalie Duval[1,2], Célia Vaslin[3,4,5,*], Tiago C. Barata[1,*], Youcef Frarma[1], Vincent Contremoulins[1,6], Xavier Baudin[1,6], Stéphane Nedelec[3,4,5,‡] and Vanessa C. Ribes[1,‡]

ABSTRACT

Bone morphogenetic proteins (BMPs) are secreted regulators of cell fate in several developing tissues. In the embryonic spinal cord, they control the emergence of the neural crest, roof plate and distinct subsets of dorsal interneurons. Although a gradient of BMP activity has been proposed to determine cell type identity *in vivo*, whether this is sufficient for pattern formation *in vitro* is unclear. Here, we demonstrate that exposure to BMP4 initiates distinct spatial dynamics of BMP signalling within the self-emerging epithelia of both mouse and human pluripotent stem cell-derived spinal organoids. The pattern of BMP signalling results in the stereotyped spatial arrangement of dorsal neural tube cell types, and concentration, timing and duration of BMP4 exposure modulate these patterns. Moreover, differences in the duration of competence time-windows between mouse and human account for the species-specific tempo of neural differentiation. Together, this study describes efficient methods for generating patterned subsets of dorsal interneurons in spinal organoids and supports the conclusion that graded BMP activity orchestrates the spatial organization of the dorsal neural tube cellular diversity in mouse and human.

KEY WORDS: Bone morphogenetic proteins, Patterning, Organoid, Relay and associating spinal dorsal interneurons, Pluripotent stem cells differentiation, Self-organization

INTRODUCTION

The rise of methods to generate pluripotent stem cell (PSC)-derived organoids containing multiple cellular subtypes arrayed in three-dimensional (3D) structures has opened new avenues to decipher the principles underlying the emergence of patterns of differentiation (Huch et al., 2017; Trujillo and Muotri, 2018). These patterns are likely to be established in response to chemical and mechanical cues applied through culture medium and generated by the endogenous cellular diversity. However, the mechanisms by which organoid cells interpret these cues and acquire specific cell fates largely remain to be determined.

To gain insight into these mechanisms, we focused on cellular subtypes generated in the dorsal part of the embryonic spinal cord. The spinal cord originates from the caudal lateral epiblast (CLE) that transits through a pre-neural (PNP) state before acquiring a neurogenic progenitor (NP) state (Henrique et al., 2015). Acquisition of the CLE and PNP states depends on the combined activity of fibroblast growth factor (FGF) and Wnt signalling, while the transition to the NP state is promoted by retinoic acid (RA) signalling. NPs are then directed towards specific neurogenic programmes, depending on their position along the dorso-ventral (D-V) axis of the neural tube (Fig. 1A) (Kalcheim, 2018; Lai et al., 2016). In the dorsal neural tube, NPs comprise six discrete cell types, named from dorsal to ventral as dp1 to dp6 NPs, as well as a group of very dorsal cells that gives rise to neural crest cells (NCCs) and the roof plate (RP) (Fig. 1A). dp4 to dp6 NPs differentiate into five associating interneuron (IN) subtypes: the early born dI4 to dI6 and the late born dILA and dILB. dp1 to dp3 NPs generate dI1 to dI3 relay INs. These neurons form functional circuits, in which associating INs transmit the information coming from NCC-derived peripheral sensory neurons to relay sensory spinal IN that in turn convey this information to the brain.

The commitment of NPs towards these dorsal fates is determined by specific combinations of transcription factors (TFs) that display stereotypic temporal and spatial expression profiles (Fig. 1A) (Kalcheim, 2018; Lai et al., 2016). The profiles of TFs that mark the NCCs, RP and dp1 to dp3 NPs are, in part, generated in response to gradients of diffusing bone morphogenetic proteins (BMPs) (Kalcheim, 2018; Le Dréau and Martí, 2013; Zagorski et al., 2017). Classical developmental studies led to the model in which the concentration, duration and timing of exposure to BMP are interpreted by PNP and NP cells, guiding them towards a specific fate. Exposing PNP cells explanted from chick embryos to increasing BMP4 concentrations or longer incubations triggers a progressive dorsalization of the generated cell types (Liem et al., 1995; Sasai et al., 2014; Tozer et al., 2013). The emergence of distinct cell fates through modulating BMP receptor activity within chick embryo NPs indicated that *in vivo* BMP signalling levels may also provide positional information (Timmer et al., 2002; Zechner et al., 2003). Similarly, inhibiting BMP signalling using the antagonist Smad6 at discrete developmental stages reinforced the idea that the duration of BMP signalling discriminates between dorsal cell types (Tozer et al., 2013). Moreover, PNP cells harbour time-regulated competence for dorsal fate specification in response to BMP: the ability of PNP cells to generate NCCs in response to BMP4 being limited in time (Nitzan et al., 2016; Sasai et al., 2014).

However, recent work based on PSC-derived spinal organoids has questioned the morphogenetic potential of BMP (Andrews et al., 2017; Gupta et al., 2018; Meinhardt et al., 2014; Ogura et al., 2018). Exposure to BMP triggered PNP or NP dorsalization in the organoids. However, regardless of the concentration of BMP used,

[1]Institut Jacques Monod, CNRS UMR7592, Université Paris Diderot, Sorbonne Paris Cité, 75205 Paris Cedex, France. [2]Institut Pasteur, Department of Developmental and Stem Cell Biology, CNRS URA 2578, 75015 Paris, France. [3]Inserm, UMR-S 1270, 75005 Paris, France. [4]Sorbonne Université, Science and Engineering Faculty, 75005 Paris, France. [5]Institut du Fer à Moulin, 75005 Paris, France. [6]ImagoSeine core facility of Institut Jacques Monod and member of France-BioImaging.
*These authors contributed equally to this work

‡Authors for correspondence (vanessa.ribes@ijm.fr; stephane.nedelec@inserm.fr)

T.C.B., 0000-0002-1483-7990; Y.F., 0000-0002-7996-195X; X.B., 0000-0002-6002-6347; S.N., 0000-0001-8044-2498; V.C.R., 0000-0001-7016-9192

Received 8 January 2019; Accepted 18 June 2019

Development (2019) 146, dev175430. doi:10.1242/dev.175430

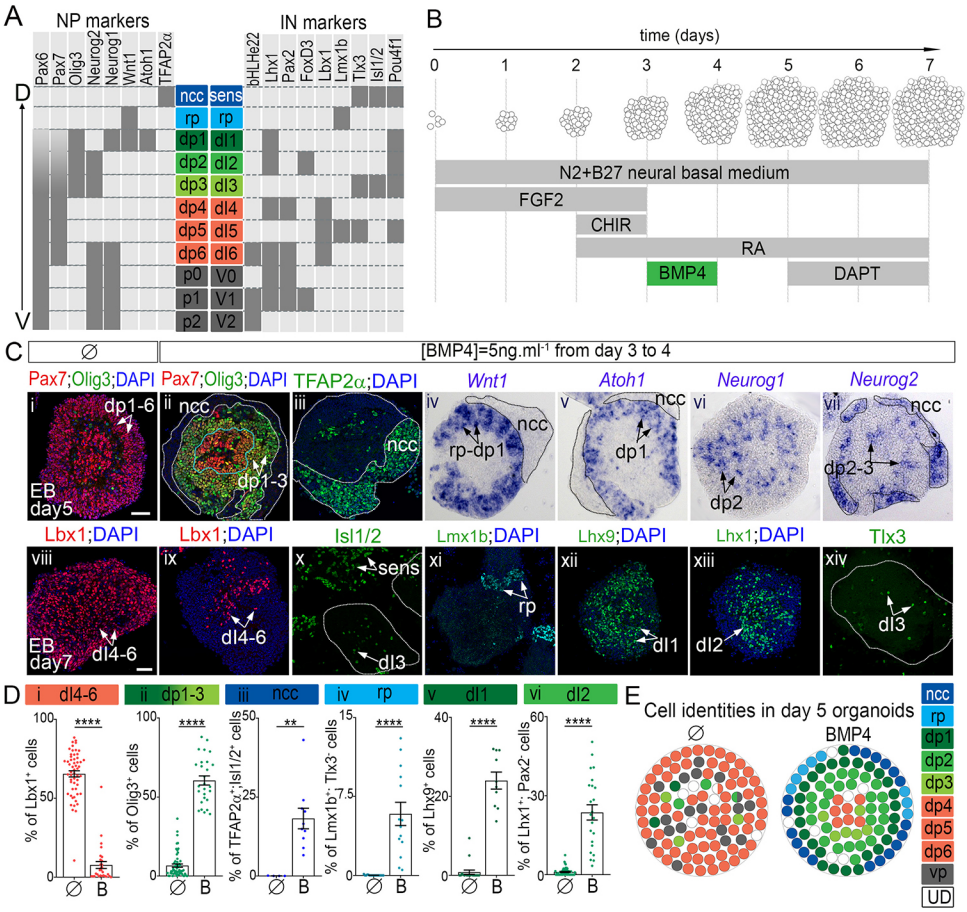

Fig. 1. BMP4 patterns mouse spinal organoids. (A) *In vivo* D-V expression patterns of neural progenitor (NP) and interneuron (IN) TF markers. (B) Schematics of differentiation conditions that generate dorsal spinal cellular subtypes in EBs. (C) Immunodetection (i-iii,viii-xiv) and *in situ* hybridization (iv-vii) for the indicated cell types. White and black outlines in ii-v,vii surround the NCC territory; blue outline in ii indicates cells less responsive to BMP4; white outlines in x and xiv indicate the EB contour. (D) Percentage of cell types harbouring the indicated TF code per image field (individual values; data are mean ±s.e.m.). $^{**}P\leq0.01$ and $^{****}P\leq0.0001$. (E) Graphs displaying the distribution and percentage of cell subtypes in day 5 organoids; white circles indicate cells with undetermined fate (UD). sens, peripheral sensory neurons. Scale bars: 60 µm.

several dorsal neural subtypes were generated in a non-organized fashion. This raised the possibility that BMP acts as a permissive, rather than an instructive, signal for the acquisition of dorsal cell fates (Andrews et al., 2017) and that additional signals or mechanisms are responsible for the *in vivo* spatial organization.

To tackle this issue, we have established robust embryoid body (EB)-based protocols to drive mouse or human PSCs into PNP cells that acquire a dp4 to dp6 state. In these EBs, BMP4 induces concentric patterns of several dorsal neural tube cell types that are reminiscent of those found along the D-V axis of the embryo. These patterns depend on the activity of the position-specific temporal profiles of the BMP transcriptional effectors Smad1, Smad5 and Smad9 within the emerging organoid epithelia. Varying the concentration, duration and timing of exposure to BMP4 modifies the cell types generated within these patterns. Furthermore, our data on human organoids revealed that, across evolution, the length of time windows for which PNP and NP cells are competent to generate discrete cell fates in response to BMP4 have been adapted to match species-specific temporal sequences of neural differentiation.

RESULTS AND DISCUSSION

Efficient generation of associating INs within spinal organoids

In order to generate dorsal spinal neurons in organoids derived from mouse embryonic stem cells (ESCs), we have adopted 3D EB-based differentiation and adapted culture conditions used for ventral spinal cells generation (Gouti et al., 2014; Maury et al., 2015; Wichterle et al., 2002). EBs were produced in neural basal medium supplemented with FGF2 for the first 3 days of culture and CHIR (CHIR99021), a GSK3 inhibitor, was used to activate Wnt signalling between day 2 and 3 (Fig. 1B). Many day 3 EB cells treated with these two compounds adopted a mesodermal fate, which could be prevented by adding the neuralizing cue RA on day 2 (Fig. 1A,B,D; data not shown) (Beccari et al., 2018; Henrique et al., 2015). CHIR drove the NPs towards caudal $Cdx2^+$ fate (Henrique et al., 2015), while FGF2 further caudalized the state of cells, as shown by the induction of brachial markers such as *Hoxc6* (Fig. S1C,D,E) (Liu et al., 2001). In line with *in vivo* studies (Alvarez-Medina et al., 2008; Lee and Deneen, 2012; Valenta et al., 2011; Zechner et al., 2003), CHIR-mediated Wnt signalling activation favoured dorsal fate acquisition, with 80% of cells exhibiting a dp4 to dp6 molecular identity (Fig. 1Ci,E, Fig. S2A,Bi-iii,C). Accordingly, at day 7, following a 48 h-long treatment with Notch signalling inhibitor DAPT (Fig. S3A), EBs contained mainly neurons expressing typical markers of the dI4 to dI6 associating INs (Fig. 1Cviii,Di, Fig. S3B,C). Thus, the identified combination of FGF2, Wnt agonist, RA and DAPT rapidly and efficiently produces mouse ESC-derived organoids containing brachial spinal associating progenitors (day 4, 5) or neurons (day 7) (Andrews et al., 2017; Meinhardt et al., 2014).

Concentric patterns of dorsal neuronal cell types formed in response to BMP4 exposure

We next examined the effects of BMP4, a BMP ligand implicated in neural patterning (Le Dréau and Martí, 2013), by exposing day 3 NPs to 5 ng ml^{-1} BMP4 for 24 h (Fig. 1B). Consistent with BMP4 being a 'dorsalizing' cue, it induced markers of NCCs, RPs, relay dp1/dI1 and dp2/dI2 cells (Fig. 1Cii-vii,ix-xiv,Dii-vi, Figs S2Biv-viii‴,C,Di, S3B). In day 4 and 5 EBs, these markers displayed

Development (2019) 146, dev175430. doi:10.1242/dev.175430

stereotyped concentric patterns of expression organized along the outer-inner axis of the organoid, with their relative position matching the one found along the D-V axis of the neural tube (Fig. 1Cii-vii,E, Fig. S2Bviii). At day 7, the sensory neurons produced from NCCs in the outer ring detached in part from the EB to colonize the dish plate (Fig. 1Cx, not shown). RP cells clustered at the EB periphery and were surrounded by dI1 INs (Fig. 1Cxi, Fig. S3B). Inside the EB, dI2 and a few dI4-6 associating INs were intermingled (Fig. 1Cix, xiii). Altogether, these data demonstrate that, in addition to creating cellular diversity, BMP4 directs spatial arrangement so that the most dorsal cell types are found at a more peripheral position than the ventral ones (Fig. 1E). As shown in the developing spinal cord (Lai et al., 2016), this organization attenuates over time owing to NCC and post-mitotic IN delamination. This may explain why the patterning activity of BMP has not been noticed in previous studies as organoids were analysed solely for terminally differentiated neurons (Andrews et al., 2017; Gupta et al., 2018; Ogura et al., 2018).

Spatial and temporal dynamics in Smad1, Smad5 and Smad9 activity triggered by BMP4 exposure

We next sought to investigate whether BMP4-mediated EB patterning could stem from differential spatial and temporal activation of its intracellular downstream effectors. For this, we monitored the levels of the phosphorylated forms of the TFs Smad1, Smad5 and Smad9 (PSmads) from day 3 to 4 in presence or absence of BMP4 (Fig. 2A-C, Fig. S4).

At all time-points, PSmads^{+} cells formed a spatially restricted, three to five cell wide ring, at the periphery of EBs. In contrast, cells deeper in the organoid were devoid of PSmads signal (Fig. 2Avi-x, B, Fig. S4A). This organization could be recapitulated by exposing EB to BMP2 (Fig. S6), but such a spatial restriction in the cell response to signalling cues was not observed for other compounds (not shown) (Maury et al., 2015). This response to BMP was not due to a difference in competence between the outer and inner cells, as single cells obtained from dissociated day 3 EBs homogeneously activated Smads in response to BMP and all cells acquired a NCC state later on (Fig. 2E). This sharp spatial organization could thus emerge from the limited rate of BMP diffusion (Kicheva et al., 2007; Pomreinke et al., 2017; Zinski et al., 2017) or stem from the emergence of a specific tissue organization within EBs. Previous work has demonstrated that the extracellular matrix separating an outer epithelium from inner epithelia can act as a barrier that hampers BMP diffusion (Hu et al., 2004; Ma et al., 2017; Perrimon et al., 2012; Plouhinec et al., 2013; Ramirez and Rifkin, 2009; Wang et al., 2008) (Fig. 2D,F). The emergence of epithelia was revealed by analysing the distribution profiles of Par3, a member of apical protein complexes, and of laminin, a component of the basal lamina (Fig. 2D, Fig. S5i-iv). PSmads^{+} cells delineated exactly the outer epithelium whose apical side faced the culture medium (Fig. 2D,F).

The analysis also revealed that P-Smads levels within the outer epithelium varied in space and time. Smads activation displayed a decreasing inward gradient across this epithelium (Fig. 2B, Fig. S4B). The gradient amplitude decreased progressively over time (Fig. 2C), except in the outer-most layer of NCC where, after the initial decline, Smads activity rose again (Fig. 2Ax,C,F, data not shown). The temporal adaptation of BMP signalling was confirmed by the progressive decrease in the levels of BMP4 target genes (Fig. 2Axv, Fig. S2Dii). Negative feedback mediated by the BMP antagonist noggin could be at stake, as its gene was transcriptionally induced 3 h after BMP4 addition, when PSmads levels had declined (Fig. 2Axi-xv) (Brazil et al., 2015). Progressive depletion of

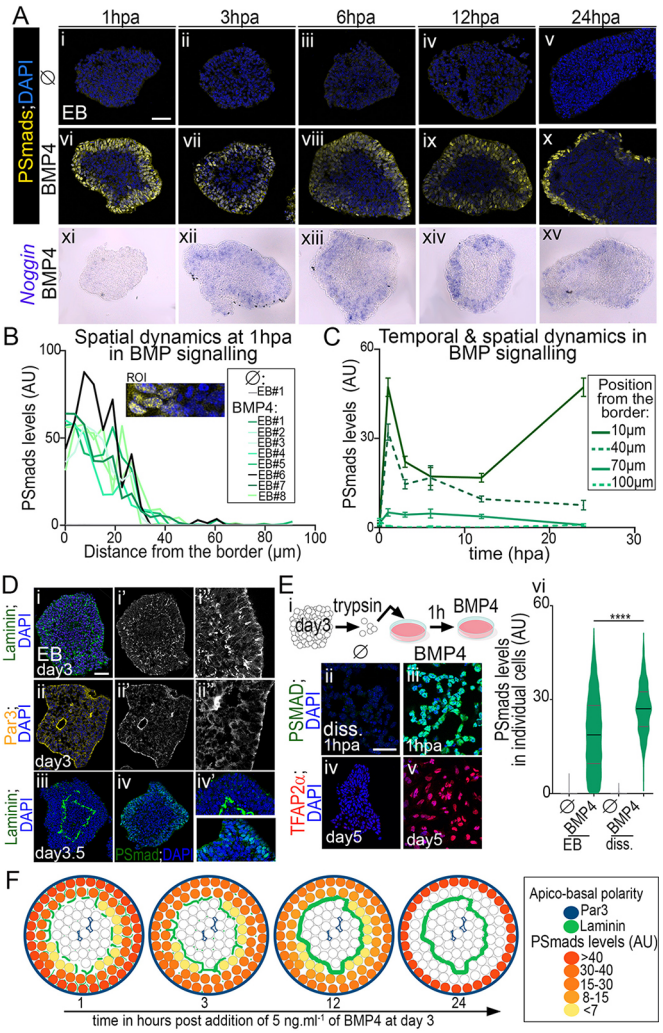

Fig. 2. Spatial and temporal dynamics of PSmads in response to BMP4. (A) Immunodetection of phospho-Smad1, Smad5 and Smad9 (PSmads), and DAPI labelling (i-x) and *in situ* hybridization against Noggin (xi-xv) in EBs cultured without or with 5 ng ml^{-1} BMP4 (added from day 3) and harvested several hours post-BMP4 addition (hpa). (B) Gradients of PSmads are measured in eight independent regions of interest (ROI; inset) 1 hpa. (C) Temporal and spatial dynamics in PSmad levels in cells at discrete distances from EB borders (data are mean±s.e.m.). (D) Laminin, Par3 and PSmad immunodetection, and DAPI labelling in day 3 and 3.5 EBs. (i′,ii′) Laminin and Par3 staining; (i″,ii″) higher magnification of i′,ii′. (E) (i) Schematics of experimental procedure used to assess the fate of dissociated cells from day 3 EBs exposed to 5 ng ml^{-1} BMP4 1 h post-dissociation. (ii-v) Immunostaining of the indicated markers in dissociated cells 1 hpa (ii,iii) or at day 5 (iv,v). (vi) PSmad levels in EBs or dissociated cells 1 hpa (violin plot; data are mean±quartiles). ****P≤0.0001. (F) Graphs representing temporal and spatial dynamics in PSmad levels and polarity markers. Scale bars: 60 µm.

receptors from the cell surface represents an alternative explanation for temporal adaptation (Miller et al., 2019). Together, these data indicate that stereotyped temporal profiles of intracellular signalling are generated in response to BMP4, according to the location of the cell within the organoid (Fig. 2C,F). This spatially graded Smad activity provides an explanation for the inability of BMP4 to drive cells in organoids towards a unique cell type (Andrews et al., 2017; Gupta et al., 2018), which creates an organized cellular diversity. Furthermore, the match between this position-specific signalling dynamics and the emergence of distinct cell types supports a model where ‘positional information’ results from

Development (2019) 146, dev175430. doi:10.1242/dev.175430

a combination of the levels and the duration of PSmads (Tozer et al., 2013).

Three tuneable morphogenetic parameters of BMP4 exposure discriminate between relay IN subtypes

To assess directly the morphogenetic potential of BMP4 in organoids, we sought to modulate the three main parameters known to influence cell response to morphogens (Sagner and Briscoe, 2017): the ligand concentration, the exposure duration and the time point at which the ligand is added (Figs S7 and S8).

Increasing BMP4 concentration increased the number of PSmads^{+} cells (Fig. S7Avi), the mean levels in PSmads (Fig. S7Avii) as well as the duration for which Smads were active (see insets in Fig. S7Aii-v). Similarly, the duration of BMP4 exposure altered the temporal dynamics of signalling. Nuclear PSmads levels fell 6 h after BMP4 removal (Fig. S7B), arguing against a long-term memory of intracellular signalling by cells exposed to BMP (Tozer et al., 2013). Importantly, the modulation of PSmad dynamics by increasing BMP4 concentration or duration extended the total amount of BMP dependent cell-types generated and promoted more dorsal cell types at the expense of more ventral ones (Fig. 3A,C,D, Fig. S8A,B).

Changing the time at which EBs were exposed to BMP4 also had strong effects on cell identities (Fig. 3B, Fig. S8C and compare Fig. 1C,D to Fig. 3D). Cells displayed a 12 h competence time window for generating specific BMP4-dependent cell types, the most dorsal cell types requiring an earliest time of exposure than more ventral ones (Fig. 3Bii-vii). This is in agreement with the limitation in time for chick spinal NP to become NCCs in response to BMP4 (Sasai et al., 2014). Importantly, the switches in cell competence were not due to alteration in the ability of a cell to transduce BMP4 information intracellularly. The amplitude (Fig. S7Cvi), gradient (insets in Fig. S7Cii-iv) and temporal adaptation (not shown) of PSmad profiles remained invariant upon shifts in the timing of BMP4 exposure. Thus, the competence could stem from changes in the molecular state of NPs during the course of their differentiation (Fig. S2Bi-vi) (Sasai et al., 2014).

Finally, in agreement with concentration, duration and timing of exposure being morphogenetic parameters (Sasai et al., 2014; Tozer et al., 2013), we determined conditions needed to generate organoids containing a dominant relay IN subpopulation at their periphery (Fig. 3C,D), including dI2 and dI3, which were poorly generated in previous protocols (Andrews et al., 2017).

Species-specific changes in NP competence time windows are related to the evolution of neuronal differentiation temporality

Dynamics of neural differentiation and tissue sizes are highly variable between species (Ebisuya and Briscoe, 2018), raising the issue of whether morphogen interpretation is modulated to scale

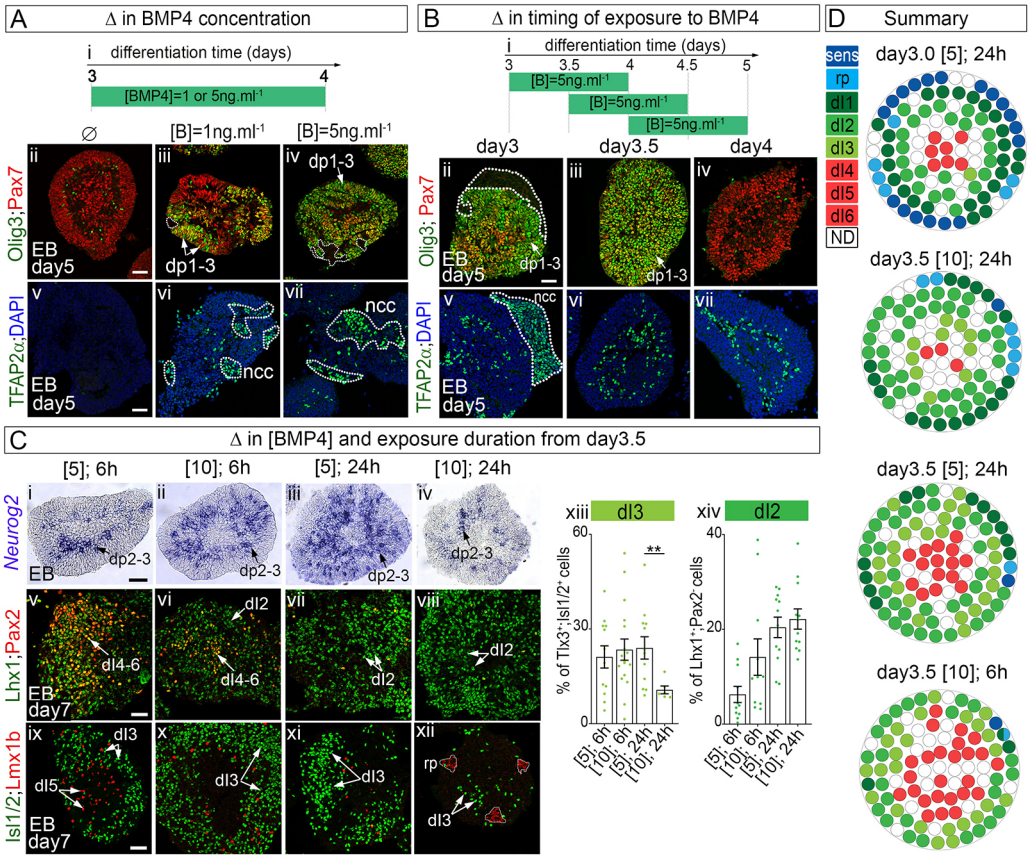

Fig. 3. Morphogenetic parameters of BMP4 exposure generate specific relay IN subtypes. Phenotypic characterization of EBs upon the modulation of BMP4 concentration (A), exposure timing (B) and both BMP4 concentration and exposure duration when adding BMP4 at day 3.5 (C). (Ai,Bi) Schematics indicating BMP4 exposure conditions. (Aii-vii,Bii-vii,Cv-xii) Immunostaining for the indicated markers in EBs grown under the indicated conditions at day 7. (Ci-iv) *In situ* hybridization for Neurog2 in day 5 EBs cultured under the indicated conditions. (Cxiii,xiv) Percentage of dI2 and dI3 INs harbouring the indicated TF code per image field (individual values; data are mean±s.e.m.). $^{**}P \leq 0.01$. (D) Graphs displaying the distribution and percentage of cell subtypes in day 7 organoids cultured under the indicated conditions. Scale bars: 60 µm.

Development (2019) 146, dev175430. doi:10.1242/dev.175430

with these dynamics. To address this, we modified our protocol to generate ventral spinal neurons from human iPSCs (Maury et al., 2015) (Fig. 4Ai). As for mouse ESCs, removing the Shh agonist SAG was sufficient to generate spinal organoids containing mostly dp4-dp6 NPs at day 9 of differentiation and associating neurons at day 14 (Fig. 4Aii,iii). Importantly, although both human and mouse dorsal spinal organoids contained similar number of cells (not shown), the time taken to generate these cells in human was around ∼2.5 times longer. Hence, as for motor neuron generation, the speed of differentiation during dorsal differentiation varies greatly between vertebrate species (Maury et al., 2015; Wichterle et al., 2002).

Exposure of hiPSC-derived organoids to BMP4 revealed that the response of human cells is similar to that of mouse cells. Smad activation was restricted to the outer layer of cells, which was separated from more inner cells by a basal lamina (Fig. 4B, Fig. S5v-viii). PSmad levels were higher in the most peripheral cells and were decreased within the width of the epithelium (Fig. 4Bi,i′). Accordingly, different cell types were produced in a concentric manner, with the most-dorsal subtypes located at a more peripheral position than the ventral subtypes (Fig. 4D). Finally, both BMP4 concentration and exposure duration influenced the proportion of the BMP-dependent cell types produced (Fig. 4D,E). As in mouse, human NPs displayed competence time windows for the generation of NCCs versus dp1-dp3 cells (Fig. 4C). Yet these windows lasted about twice as long as they did in mouse (compare Fig. 4C with 3B) and paralleled the species-specific time frames of neuronal differentiation. This supports the idea that competence is a consequence of sequential transitions in the transcriptional states of differentiating NPs that occur at slower pace in humans (Sasai et al., 2014).

Together, using efficient and rapid protocols for the differentiation of human and mouse PSC in organoids containing specific subsets of associating and relay spinal neurons, we revealed key parameters for BMP4-mediated tissue patterning. First, 3D polarized epithelia emerging within the organoids participate in the generation of stereotyped profiles of Smad activity and of discrete subsets of cellular subtypes. Their emergence constrains the spatial distribution of not only proteins controlling ligand diffusion, but also of the basolaterally located BMP receptors, which together are likely to generate spatial and temporal dynamics in BMP intracellular signalling (Etoc et al., 2016; Miller et al., 2019; Pomreinke et al., 2017; Wang et al., 2008; Zhang et al., 2018preprint). Second, as shown for a great number of morphogens (Sagner and Briscoe, 2017), the timing of differentiation, i.e. the molecular state of the receiving cells, appeared to be the most constraining parameter for the response to BMP4, with species specificities. In terms of bioengineering of BMP-dependent cell

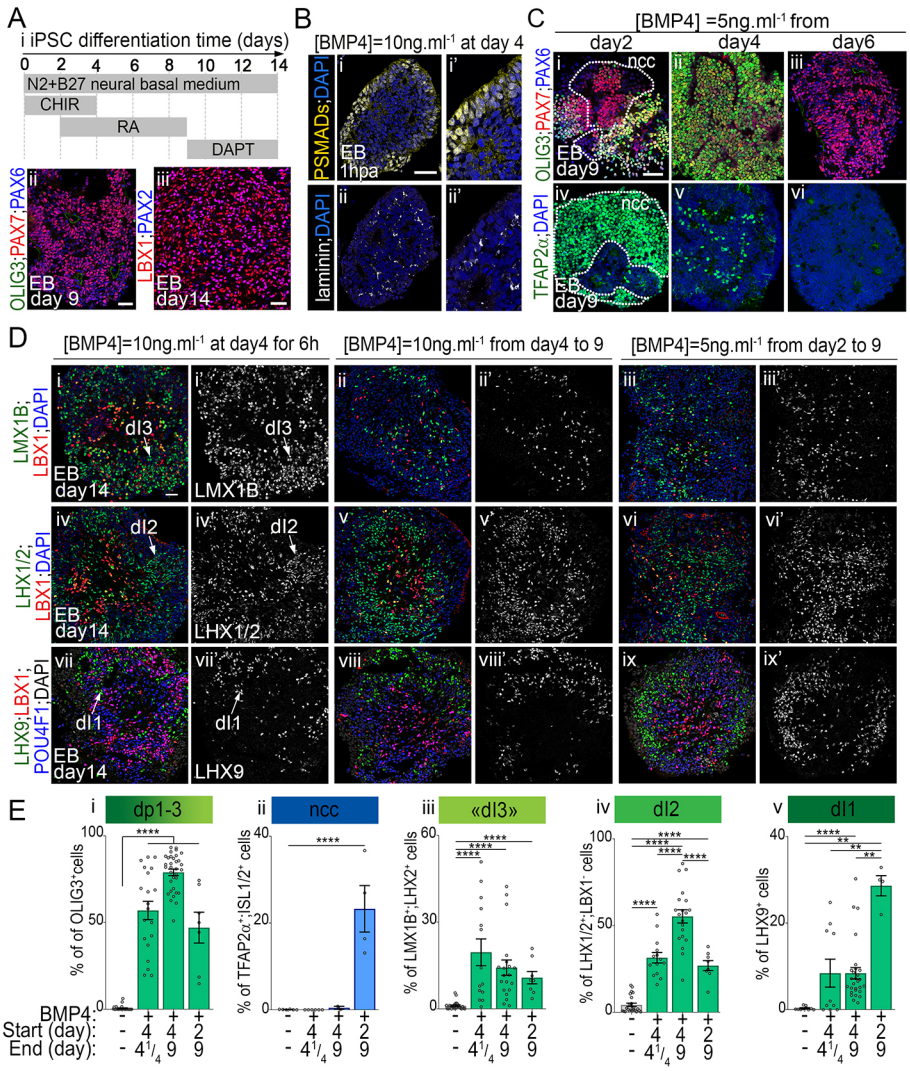

Fig. 4. Morphogenetic effects of BMP4 exposure on human iPSC-derived spinal organoids. (A) Generation of associating progenitors and IN from human iPSCs. (Ai) Schematics indicating drug treatments to convert human iPSCs into dorsal spinal cells. (Aii,iii) Immunostaining for the indicated NP (ii) and IN (iii) markers in day 9 and 14 organoids. (B) Immunodetection of pSmads or laminin and DAPI labelling in day 4 organoids treated for 1 h with BMP4. (C) Immunostaining for the indicated NP markers in day 9 EBs grown in presence of BMP4 added at the indicated time points and maintained up to day 9. (D) Immunostaining for the indicated post-mitotic markers in day 14 EBs grown under the indicated conditions. (E) Percentage of IN subtypes harbouring the indicated identities (individual values; data are mean±s.e.m.). $^{**}P\leq0.01$ and $^{****}P\leq0.0001$. Scale bars: 60 µm.

Development (2019) 146, dev175430. doi:10.1242/dev.175430

types for basic and translational perspectives, our results call for the elaboration of new diffusible BMP pathway activators to generate homogenous populations of cells and for a precise temporal control of morphogen signalling with drug treatments.

MATERIALS AND METHODS

Cell line maintenance and differentiation

Mouse ESC line HM1 (Selfridge et al., 1992) at passages ranging from 15 to 19 were maintained on mitotically inactive primary mouse embryo fibroblasts in EmbryoMax D-MEM supplemented with 10% ESC-qualified foetal bovine serum (Millipore), L-glutamine, non-essential amino acid, nucleosides, 0.1 mM β-mercaptoethanol (Life Technologies) and 1000 U ml^{-1} leukaemia inhibitory factor (Millipore). Human iPSC WTSIi008-A cell and WTSIi002-A line (EBISC, European Bank for Pluripotent Stem Cells) were cultured in E8 medium on vitronectin (Life Technologies) as previously described (Maury et al., 2015).

To initiate mouse ESC embryoid bodies differentiation, cells were trypsinized and placed twice onto gelatinized tissue culture plates to remove feeders. Cells (5×10^4 cells ml^{-1}) were placed in ultra-low attachment petri dishes (Corning) and in Advanced Dulbecco's Modified Eagle/F12 and Neurobasal media (1:1, Life Technologies) supplemented with 1× B27 devoid of vitamin A and 1×N2 (Life Technologies), 2 mM L-glutamine (Life Technologies), 0.1 mM β-mercaptoethanol, penicillin and streptomycin (Life Technologies). At this concentration of cells, small EBs were formed from day 1 of differentiation, and grown as such up to day 7 of differentiation; medium was changed every day from day 2 onwards. Human PSC EB differentiation was performed as described by Maury et al. (2015), except the medium did not contain LDN193189 or SB431542. Cells (1.5×10^5 cells ml^{-1}) were seeded in ultra-low attachment six-well plates (Corning). Medium was changed on days 2, 4, 7, 9 and 11 of differentiation. Chemical drugs to inhibit or activate key developmental signalling pathways were used at the following concentrations: 10 ng ml^{-1} bFGF (FGF2, R&D), 3 µM CHIR99021 (Tocris or Axon Medchem), 10 nM retinoic acid (Sigma), 1 ng ml^{-1} to 15 ng ml^{-1} BMP4 (R&D), 10 µM DAPT (Stemgent). Figs 1B and 4A depict the time frames over which these drugs were applied to mouse and human EBs, respectively. Human iPSC experiments were declared (CD-2015-2559) and approved by local ethical Committee (CPP A95).

Dissociation of mouse ESC-derived neuroprogenitors for monolayer culture

EB at day 3 of differentiation were incubated with 0.05% trypsin-EDTA for 3 min. After fetal bovine serum (FBS) trypsin inactivation they were dissociated by pipetting and filtered (40 µm pore size). Single cell suspensions were plated at 10^5 cells $well^{-1}$ in a 24-well plate onto a glass coverslip coated with 20 µg ml^{-1} poly-ornithine (Sigma) and 5 µg ml^{-1} laminin (Life Technologies). Cells were allowed to adhere 1 h before the addition of fresh differentiation medium containing BMP4.

Expression analyses

RT-qPCR

Total RNA was extracted from 50 to 250 EBs collected at different time points using the NucleoSpin RNA kit (Macherey-Nagel) following manufacturer's instructions. cDNAs were synthetized using SuperScript IV (Thermo Fisher Scientific), random primers and oligo dT. For real-time quantitative PCR (RT-qPCR), SYBR Green I Master (Roche) and the LightCycler 480 II (Roche) were used. PCR primers were designed using Primer3 software (Table S1). Levels of expression per gene for a given time point was measured in biological duplicates or triplicates. Mouse gene expression levels were expressed relatively to TATA-box binding protein (TBP) mRNA levels and normalized to the expression in either GD11.5 dissected spinal cord or mouse ESCs.

Immunofluorescence and *in situ* hybridization

EB fixation, embedding and cryosectioning have been described previously (Maury et al., 2015), so have the immunolabelling and *in situ* hybridization protocols (Briscoe et al., 2000; Yamada et al., 1993). Details of the antibodies are provided in Table S2. Analyses were carried out using a Leica TCS SP5 confocal microscope or a Zeiss Axioplan 2, and images processed with Photoshop 7.0 software (Adobe Systems) or ImageJ v.1.43g image analysis software (NIH).

Quantification

The number of cells immunolabelled was calculated using Cell Profiler (Broad institute) after nuclei segmentation based on DAPI fluorescence signal with a signal intensity threshold and was expressed as the percentage of all detected nuclei. The EB area labelled by *in situ* hybridization probes was estimated using ImageJ v.1.43g image analysis software (NIH) and was expressed as the percentage of the whole EB surface. For each condition, these quantifications were performed on a minimum of five images per experiment and on a minimum of two independent experiments. Percentage of all cellular subtypes analysed were represented using a dot plot shaped as a circle; the position of the cellular subtypes reflected our observations. Levels of PSmad fluorescent signal intensity per cells were evaluated using Cell Profiler by subtracting background values from EBs that were not treated with BMP4. Violin plots were used to show the spread of these levels in five images per experiments and on a minimum of three independent experiments. The fluorescence intensity of PSmad expression along the EB outer-inner axis was measured in rectangles 16 µm wide and 100 µm long positioned perpendicular to an EB tangent line using ImageJ v.1.43g. Background measurements were obtained from EBs not treated with BMP4 and these were subtracted from each assayed profile. Statistical analysis was carried out and graphs were created using Prism Graphpad software. Non-parametric *t*-tests were used to evaluate pair-wise comparisons between conditions. *P*-values are: $*P\leq0.05$, $**P\leq0.01$, $***P\leq0.001$ and $****P\leq0.0001$.

Whole-mount immunolabelling, 3D scans and image processing

EBs fixed in 4% paraformaldehyde and rinsed with PBS were incubated in a blocking solution of 0.5% Triton X-100 and 1% BSA for 10 h. They were then incubated for 48 h with anti-PSmad antibodies (Table S2). After overnight washes in PBS and 0.5% Triton X-100, they were incubated overnight with a secondary antibody coupled to Alexa A488 (Table S2). After 1 day of washes in PBS and 0.5% Triton X-100, they were mounted in Vectashield mounting medium (Vector) between coverslips and a glass slide. They were imaged using a Leica TCS SP5 confocal microscope and the image segmentation and signal quantification were processed using Imaris (Bitplane). Notably, surfaces delimitating PSmad-positive nuclei in the EBs were defined using the surface segmentation tool (Fig. S4Ai-i″). Segmentation of PSmad-positive cells was established and the mean intensity values colour coded using the spot detection tool (Fig. S4B). All observations were carried out on at least seven EBs.

Acknowledgements

We deeply thank C. Birchmeier, T. Müller, J. B. Brunet and A. Pierani for antibodies; E. Marti and G. Le Dréau for constructs; and the ImagoSeine core facility of Institut Jacques Monod, a member of France-BioImaging (ANR-10-INBS-04) and certified IBiSA, as well as the IFM imaging facility. We are grateful to Line Manceau, Benoit Sorre and James Briscoe for critical comments on the manuscript.

Competing interests

The authors declare no competing or financial interests.

Author contributions

Conceptualization: N.D., S.N., V.C.R.; Methodology: N.D., C.V., T.C.B., Y.F., X.B., S.N., V.C.R.; Software: V.C.; Validation: N.D., C.V., T.C.B., V.C.R.; Formal analysis: N.D., C.V., T.C.B., Y.F., V.C., V.C.R.; Investigation: N.D., C.V., T.C.B., V.C.R.; Writing - original draft: V.C.R.; Writing - review & editing: N.D., C.V., S.N., V.C.R.; Visualization: V.C.; Supervision: S.N., V.C.R.; Funding acquisition: S.N., V.C.R.

Funding

S.N. and V.C.R. are Institut National de la Santé et de la Recherche Médicale researchers; N.D. is employed by the Institut Pasteur. Work in the lab of V.R. is supported by a Centre National pour la Recherche Scientifique/Institut National de la Santé et de la Recherche Médicale ATIP-AVENIR program, as well as by a Ligue Nationale Contre le Cancer grant (PREAC2016.LCC). Studies in the lab of S.N. are funded by an Institut National de la Santé et de la Recherche Médicale ATIP-

AVENIR program co-sponsored by the Association Française contre les Myopathies (AFM-telethon) and a chair of excellence of the Laboratoire d'Excellence de Biologie pour la Psychiatrie (Bio-Psy) (11-LABX-0035).

Supplementary information

Supplementary information available online at
http://dev.biologists.org/lookup/doi/10.1242/dev.175430.supplemental

References

Alvarez-Medina, R., Cayuso, J., Okubo, T., Takada, S. and Marti, E. (2008). Wnt canonical pathway restricts graded Shh/Gli patterning activity through the regulation of Gli3 expression. *Development* **135**, 237-247. doi:10.1242/dev.012054

Andrews, M. G., del Castillo, L. M., Ochoa-bolton, E., Yamauchi, K., Smogorzewski, J., Butler, S. J., Castillo, L. M., Ochoa-bolton, E., Yamauchi, K., Smogorzewski, J. et al. (2017). BMPs direct sensory interneuron identity in the developing spinal cord using signal-specific not morphogenic activities. *eLife* **6**, e30647. doi:10.7554/eLife.30647

Beccari, L., Moris, N., Girgin, M., Turner, D. A., Baillie-Johnson, P., Cossy, A.-C., Lutolf, M. P., Duboule, D. and Arias, A. M. (2018). Multi-axial self-organization properties of mouse embryonic stem cells into gastruloids. *Nature* **562**, 272-276. doi:10.1038/s41586-018-0578-0

Brazil, D. P., Church, R. H., Surae, S., Godson, C. and Martin, F. (2015). BMP signalling: agony and antagony in the family. *Trends Cell Biol.* **25**, 249-264. doi:10.1016/j.tcb.2014.12.004

Briscoe, J., Pierani, A., Jessell, T. M. and Ericson, J. (2000). A homeodomain protein code specifies progenitor cell identity and neuronal fate in the ventral neural tube. *Cell* **101**, 435-445. doi:10.1016/S0092-8674(00)80853-3

Ebisuya, M. and Briscoe, J. (2018). What does time mean in development? *Development* **145**, dev164368. doi:10.1242/dev.164368

Etoc, F., Metzger, J., Ruzo, A., Kirst, C., Yoney, A., Ozair, M. Z., Brivanlou, A. H. and Siggia, E. D. (2016). A balance between secreted inhibitors and edge sensing controls gastruloid self-organization. *Dev. Cell* **39**, 302-315. doi:10.1016/j.devcel.2016.09.016

Gouti, M., Tsakiridis, A., Wymeersch, F. J., Huang, Y., Kleinjung, J., Wilson, V. and Briscoe, J. (2014). In vitro generation of neuromesodermal progenitors reveals distinct roles for wnt signalling in the specification of spinal cord and paraxial mesoderm identity. *PLoS Biol.* **12**, e1001937. doi:10.1371/journal.pbio.1001937

Gupta, S., Sivalingam, D., Hain, S., Makkar, C., Sosa, E., Clark, A. and Butler, S. J. (2018). Deriving dorsal spinal sensory interneurons from human pluripotent stem cells. *Stem Cell Rep.* **10**, 390-405. doi:10.1016/j.stemcr.2017.12.012

Henrique, D., Abranches, E., Verrier, L. and Storey, K. G. (2015). Neuromesodermal progenitors and the making of the spinal cord. *Development* **142**, 2864-2875. doi:10.1242/dev.119768

Hu, Q., Ueno, N. and Behringer, R. R. (2004). Restriction of BMP4 activity domains in the developing neural tube of the mouse embryo. *EMBO Rep.* **5**, 734-739. doi:10.1038/sj.embor.7400184

Huch, M., Knoblich, J. A., Lutolf, M. P. and Martinez-arias, A. (2017). The hope and the hype of organoid research. *Development* **144**, 938-941. doi:10.1242/dev.150201

Kalcheim, C. (2018). Neural crest emigration: from start to stop. *Genesis* **56**, e23090. doi:10.1002/dvg.23090

Kicheva, A., Pantazis, P., Bollenbach, T., Kalaidzidis, Y., Bittig, T., Julicher, F. and Gonzalez-Gaitan, M. (2007). Kinetics of morphogen gradient formation. *Science* **315**, 521-525. doi:10.1126/science.1135774

Lai, H. C., Seal, R. P. and Johnson, J. E. (2016). Making sense out of spinal cord somatosensory development. *Development* **143**, 3434-3448. doi:10.1242/dev.139592

Le Dréau, G. and Martí, E. (2013). The multiple activities of BMPs during spinal cord development. *Cell. Mol. Life Sci.* **70**, 4293-4305. doi:10.1007/s00018-013-1354-9

Lee, H. K. and Deneen, B. (2012). Daam2 is required for dorsal patterning via modulation of canonical Wnt signaling in the developing spinal cord. *Dev. Cell* **22**, 183-196. doi:10.1016/j.devcel.2011.10.025

Liem, K. F., Tremml, G., Roelink, H. and Jessell, T. M. (1995). Dorsal differentiation of neural plate cells induced by BMP-mediated signals from epidermal ectoderm. *Cell* **82**, 969-979. doi:10.1016/0092-8674(95)90276-7

Liu, J.-P., Laufer, E. and Jessell, T. M. (2001). Assigning the positional identity of spinal motor neurons: rostrocaudal patterning of Hox-c expression by FGFs, Gdf11, and retinoids. *Neuron* **32**, 997-1012. doi:10.1016/S0896-6273(01)00544-X

Ma, M., Cao, X., Dai, J. and Pastor-Pareja, J. C. (2017). Basement membrane manipulation in Drosophila wing discs affects Dpp retention but not growth mechanoregulation. *Dev. Cell* **42**, 97-106.e4. doi:10.1016/j.devcel.2017.06.004

Maury, Y., Côme, J., Piskorowski, R. A., Salah-Mohellibi, N., Chevaleyre, V., Peschanski, M., Martinat, C. and Nedelec, S. (2015). Combinatorial analysis of developmental cues efficiently converts human pluripotent stem cells into multiple neuronal subtypes. *Nat. Biotechnol.* **33**, 89-96. doi:10.1038/nbt.3049

Meinhardt, A., Eberle, D., Tazaki, A., Ranga, A., Niesche, M., Wilsch-Bräuninger, M., Stec, A., Schackert, G., Lutolf, M. and Tanaka, E. M. (2014). 3D reconstitution of the patterned neural tube from embryonic stem cells. *Stem Cell Rep.* **3**, 987-999. doi:10.1016/j.stemcr.2014.09.020

Miller, D. S. J., Schmierer, B. and Hill, C. S. (2019). TGF-β family ligands exhibit distinct signaling dynamics that are driven by receptor localization. *J. Cell Sci.* **146**, jcs.234039. doi:10.1242/jcs.234039

Nitzan, E., Avraham, O., Kahane, N., Ofek, S., Kumar, D. and Kalcheim, C. (2016). Dynamics of BMP and Hes1/Hairy1 signaling in the dorsal neural tube underlies the transition from neural crest to definitive roof plate. *BMC Biol.* **14**, 23. doi:10.1186/s12915-016-0245-6

Ogura, T., Sakaguchi, H., Miyamoto, S. and Takahashi, J. (2018). Three-dimensional induction of dorsal, intermediate and ventral spinal cord tissues from human pluripotent stem cells. *Development* **145**, dev162214. doi:10.1242/dev.162214

Perrimon, N., Pitsouli, C. and Shilo, B.-Z. (2012). Signaling mechanisms controlling cell fate and embryonic patterning. *Cold Spring Harb. Perspect. Biol.* **4**, a005975. doi:10.1101/cshperspect.a005975

Plouhinec, J.-L., Zakin, L., Moriyama, Y. and De Robertis, E. M. (2013). Chordin forms a self-organizing morphogen gradient in the extracellular space between ectoderm and mesoderm in the Xenopus embryo. *Proc. Natl. Acad. Sci. USA* **110**, 20372-20379. doi:10.1073/pnas.1319745110

Pomreinke, A. P., Soh, G. H., Rogers, K. W., Bergmann, J. K., Bläßle, A. J. and Müller, P. (2017). Dynamics of BMP signaling and distribution during zebrafish dorsal-ventral patterning. *eLife* **6**, e25861. doi:10.7554/eLife.25861

Ramirez, F. and Rifkin, D. B. (2009). Extracellular microfibrils: contextual platforms for TGFβ and BMP signaling. *Curr. Opin. Cell Biol.* **21**, 616-622. doi:10.1016/j.ceb.2009.05.005

Sagner, A. and Briscoe, J. (2017). Morphogen interpretation: concentration, time, competence, and signaling dynamics. *Wiley Interdiscip. Rev. Dev. Biol.* **6**, e271. doi:10.1002/wdev.271

Sasai, N., Kutejova, E. and Briscoe, J. (2014). Integration of signals along orthogonal axes of the vertebrate neural tube controls progenitor competence and increases cell diversity. *PLoS Biol.* **12**, e1001907. doi:10.1371/journal.pbio.1001907

Selfridge, J., Pow, A. M., McWhir, J., Magin, T. M. and Melton, D. W. (1992). Gene targeting using a mouse HPRT minigene/HPRT-deficient embryonic stem cell system: inactivation of the mouse ERCC-1 gene. *Somat. Cell Mol. Genet.* **18**, 325-336. doi:10.1007/BF01235756

Timmer, J. R., Wang, C. and Niswander, L. (2002). BMP signaling patterns the dorsal and intermediate neural tube via regulation of homeobox and helix-loop-helix transcription factors. *Development* **129**, 2459-2472.

Tozer, S., Le Dréau, G., Marti, E., Briscoe, J. and Le Dreau, G. (2013). Temporal control of BMP signalling determines neuronal subtype identity in the dorsal neural tube. *Development* **140**, 1467-1474. doi:10.1242/dev.090118

Trujillo, C. A. and Muotri, A. R. (2018). Brain organoids and the study of neurodevelopment. *Trends Mol. Med.* **24**, 982-990. doi:10.1016/j.molmed.2018.09.005

Valenta, T., Gay, M., Steiner, S., Draganova, K., Zemke, M., Hoffmans, R., Cinelli, P., Aguet, M., Sommer, L. and Basler, K. (2011). Probing transcription-specific outputs of beta-catenin in vivo. *Genes Dev.* **25**, 2631-2643. doi:10.1101/gad.181289.111

Wang, X., Harris, R. E., Bayston, L. J. and Ashe, H. L. (2008). Type IV collagens regulate BMP signalling in Drosophila. *Nature* **455**, 72-77. doi:10.1038/nature07214

Wichterle, H., Lieberam, I., Porter, J. A. and Jessell, T. M. (2002). Directed differentiation of embryonic stem cells into motor neurons. *Cell* **110**, 385-397. doi:10.1016/S0092-8674(02)00835-8

Yamada, T., Pfaff, S. L., Edlund, T. and Jessell, T. M. (1993). Control of cell pattern in the neural tube: motor neuron induction by diffusible factors from notochord and floor plate. *Cell* **73**, 673-686. doi:10.1016/0092-8674(93)90248-O

Zagorski, M., Tabata, Y., Brandenberg, N., Lutolf, M. P., Tkačik, G., Bollenbach, T., Briscoe, J. and Kicheva, A. (2017). Decoding of position in the developing neural tube from antiparallel morphogen gradients. *Science* **356**, 1379-1383. doi:10.1126/science.aam5887

Zechner, D., Fujita, Y., Hülsken, J., Müller, T., Walther, I., Taketo, M. M., Crenshaw, E. B., Birchmeier, W. and Birchmeier, C. (2003). β-Catenin signals regulate cell growth and the balance between progenitor cell expansion and differentiation in the nervous system. *Dev. Biol.* **258**, 406-418. doi:10.1016/S0012-1606(03)00123-4

Zhang, Z., Zwick, S., Loew, E., Grimley, J. S. and Ramanathan, S. (2018). Embryo geometry drives formation of robust signaling gradients through receptor localization. *bioRxiv*, 491290. doi:10.1101/491290

Zinski, J., Bu, Y., Wang, X., Dou, W., Umulis, D. and Mullins, M. C. (2017). Systems biology derived source-sink mechanism of bmp gradient formation. *eLife* **6**, e22199. doi:10.7554/eLife.22199

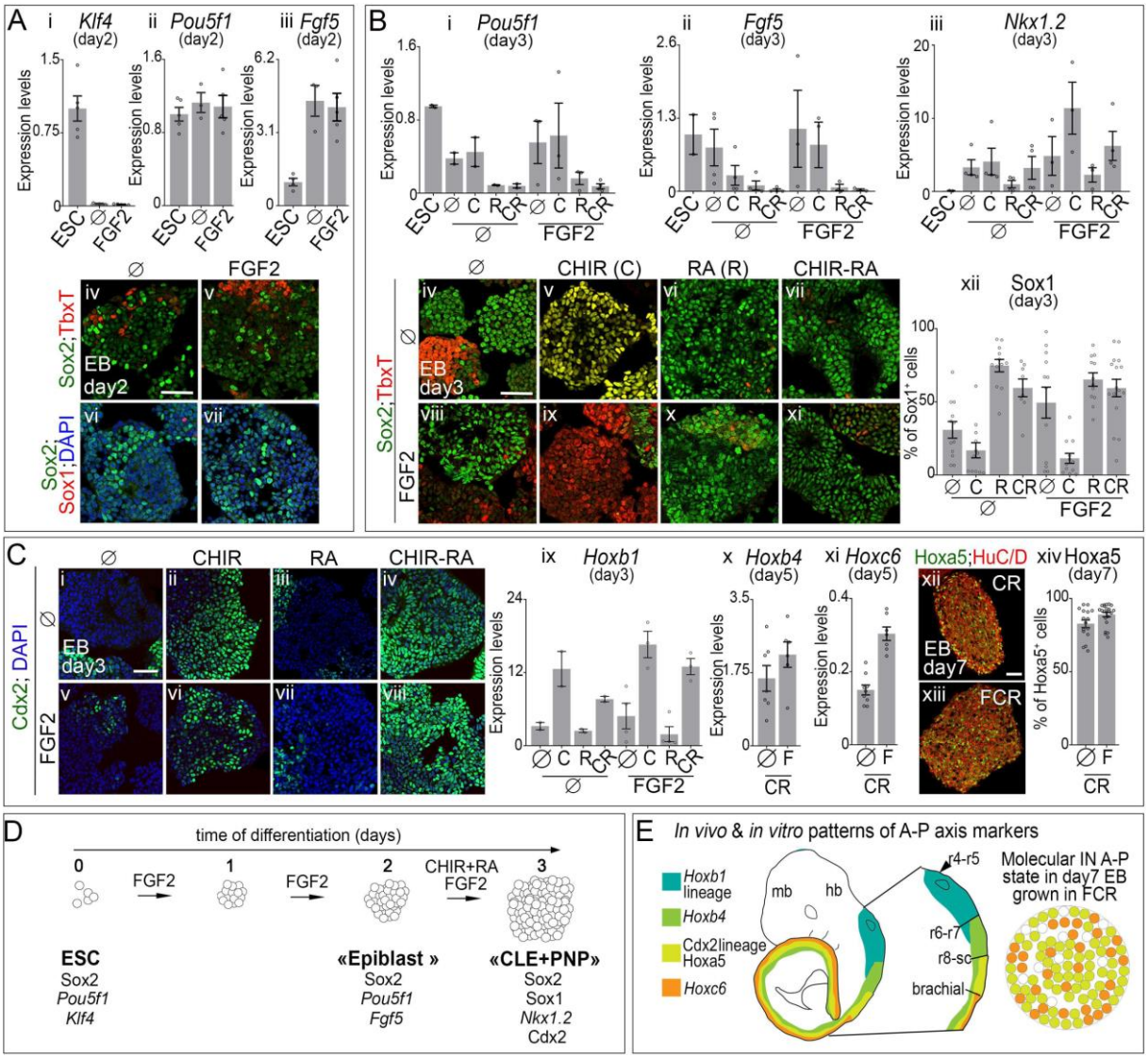

Fig. S1: FGF2, CHIR and RA impact on neural and caudal states of mouse ESC derived EB

(A)(Ai-iii) Levels of pluripotency markers *Klf4*, *Pou5f1* (*Oct4*), and *Fgf5* expression in ESC or in EB on their 2nd day of differentiation grown without any supplementation (∅) or with FGF2, quantified by RT-qPCR relative to *TBP* and normalized to their levels in ESC (circles: individual values, bars: mean±s.e.m.). **(Aiv-vii)** DAPI labelling and immuno-detection of TbxT, Sox2, and Sox1 in EB after two days in the indicated media. Scale bar: 60µM. By the 2nd day of differentiation, EB cells lost their *Pou5f1*$^{+}$;*Klf4*$^{+}$ pluripotency state, acquired epiblast molecular traits *(Pou5f1*$^{+}$;*Fgf5*$^{+}$;Sox2^{+}*)* and barely expressed specific lineage markers, such as Sox1 (neural) and TbxT (mesodermal).

(B) (Bi-iii) Expression levels of *Pou5f1*, *Fgf5* and *Nkx1.2* in ESC or in EB on their 3rd day of differentiation quantified by RT-qPCR relative to *TBP* and normalized to their levels in ESC in i and to levels in the tail bud of mouse embryos at gestational day (G.D.) 8.5 in ii and iii (circles: individual values, bars: mean±s.e.m.). **(Biv-xi)** DAPI labelling and immuno-detection of TbxT and Sox2 in EB after three days in the indicated media. Scale bar: 60µM. **(Bxii)** Quantification of $Sox1^+$ cells grown in the indicated media at day 3 (circles: individual values, bars: mean±s.e.m.). RA promoted the transition from an epiblast state to a neural state ($Sox1^+$; $Sox2^+$) and inhibited the synergic induction of the mesodermal marker TbxT by FGF2 and CHIR. Cells which are not differentiated may harbour a *Nkx1.2*$^+$ CLE state. These results are in line with several studies looking into the role of FGF and Wnt signalling during the establishment of caudal epiblast state (Beccari et al., 2018; Henrique et al., 2015).

(C)(Ci-viii) DAPI staining and immuno-detection of Cdx2 after 3 days of differentiation in the indicated media. Scale bar: 60µM**. (Cix,x,xiv)** Levels of *Hoxb1*, *Hoxb4* and *Hoxc6* quantified by RT-qPCR, relative to *TBP* expression and normalized to their levels in the spinal cord of G.D.11.5 mouse embryos in the indicated media and at the indicated stage of differentiation (circles: individual values, bars: mean±s.e.m.). **(Cxi-xiii)** Immuno-detection of Hoxa5 and HuC/D in the indicated conditions at day7 and quantification of the percentage of $Hoxa5^+$ cells per image field (circles: individual values, bars: mean±s.e.m.; scale bar: 60µM). C, R, F stand for CHIR, RA and FGF2, respectively.

CHIR triggered the caudalization of cells marked by the combined induction of Cdx2, *Hoxb1*, *Hoxb4*, Hoxa5 and *Hoxc6*, FGF2 increased *Hoxc6* expression. The molecular identities displayed by cells during the course of their differentiation [$Cdx2^+$ at day3, *Hoxb4*$^+$;*Hoxc6*$^+$ at day5 and $Hoxa5^+$ at day 7] in presence of FGF2, CHIR and RA indicate that they are driven towards a cervical-brachial state (Britz et al., 2015; Dasen et al., 2005). This is consistent with previous work demonstrating that FGF signalling is sufficient to caudalize the nervous system (e.g. (Liu et al., 2001).

(D) Schematics showing the state transitions of EB cells grown in presence of FGF2 between day0 and 3, CHIR and RA between day 2 and 3.

(E) Schematics showing the expression profiles of *Hoxb4*, *Hoxa5* and of *Hoxc6*, as well as the position of cells that had have expressed *Hoxb1* and Cdx2 in GD9.5 mouse embryos. Representation of day 7 EB grown in presence of FGF2 between day 0 and 3, CHIR and RA between day 2 and 3 inferred from data presented in C. Cells in EB grown in these conditions harboured an antero-posterior (A-P) state reminiscent of that found at the cervical-brachial levels of embryos.

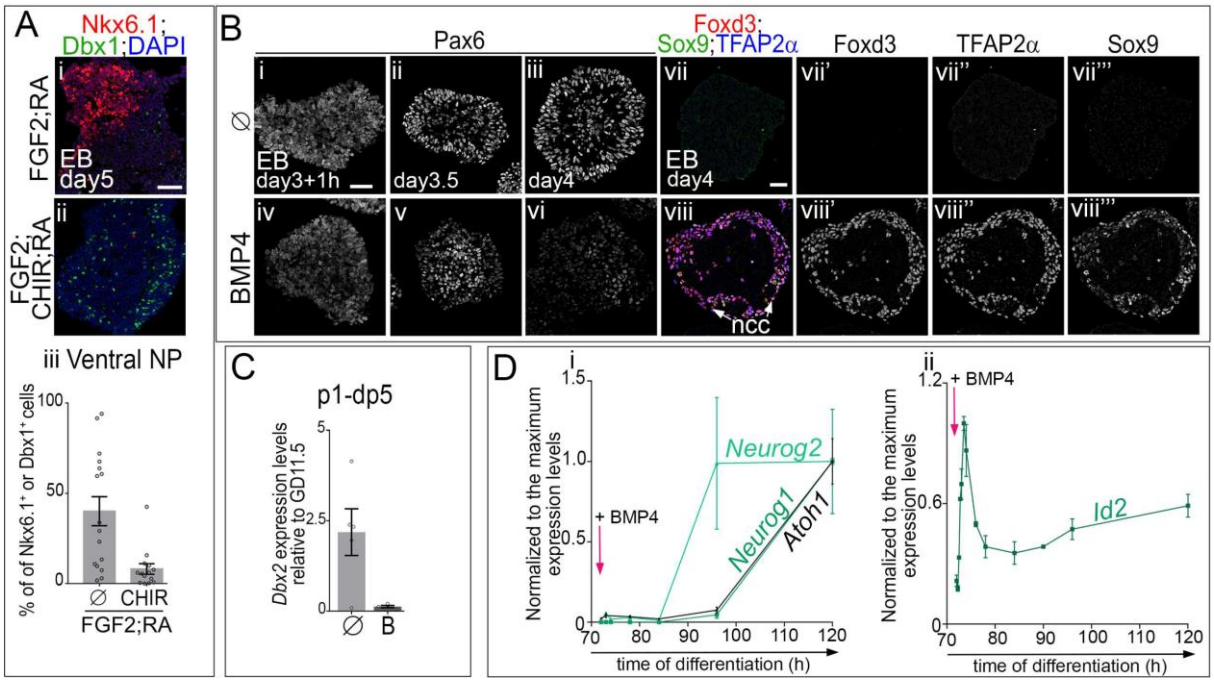

Fig. S2: Temporal and spatial dynamics in NP markers expression within dorsal spinal organoids

(A) Immuno-detection of Nkx6.1 and Dbx1 and DAPI labelling on day 5 EB cultured with FGF2 and RA with (ii) or without (i) CHIR (scale bar: 60µM) and quantification of the proportion of cells expressing either Nkx6.1 or Dbx1 per image field (circles: individual values, bars: mean±s.e.m.). CHIR mediated Wnt signalling activation dorsalised the states of NP in mouse derived EB, as shown by Nkx6.1 downregulation when CHIR is introduced in the culture medium.

(B-C) Immuno-detection of Pax6 or TFAP2β, Sox9, Foxd3 and DAPI labelling on EB at the indicated stages (B; scale bars: 60µM) and expression levels of *Dbx2*, a p1 to dp5 progenitor marker, assessed by RT-qPCR and normalized to its expression levels in G.D.11.5 mouse spinal cord in day5 EB (C). In these experiments EB were grown with FGF2, CHIR and RA without (Ø) or with (B) 5ng.ml^{-1} of BMP4 between day 3 and 4 of culture. Without BMP4 Pax6 expression increased between day3 and day3.5 suggesting that NP have acquired a new differentiated state; this could underpin the loss in the ability of cells to acquire a ncc state upon BMP4 exposure from day3.5 (i-iii, see Fig. 4B). In presence of BMP4, Pax6 levels decreased at the periphery of the EB as soon as 12hour post BMP4 addition (12hpa of BMP4), which is in agreement with cells acquiring a more dorsal fate (iv-vi, see Fig. 1A). In presence of BMP4 on day3 of differentiation cells at the periphery of the EB adopted a TFAP2β^{+};Foxd3^{+}; Sox9^{+}

ncc fate on day4, the presence of Foxd3 excluded the possibility that these cells were reminiscent to the pre-placodal ectodermal cells (Moody and LaMantia, 2015). The intermediate dorsal spinal cord marker *Dbx2* was present in day5 EB grown in absence of BMP4 which is in agreement with most EB cells that have adopted a dp4-dp6 fate. Its expression decreased upon BMP4 treatment.

(D) Expression levels of *Neurog2* (pale green line in i), *Neurog1* (dark green line in i), *Atoh1* (black line in i) and *Id2* (ii) assessed by RT-qPCR from day 3 to day 5 in EB cultured as in Fig. 1A with BMP4. In presence of BMP4, cells first induced the dp2/dp3 marker *Neurog2* before expressing the dp1 and dp2 markers *Atoh1* and *Neurog1*. This temporal sequence is similar to that found in vivo in cells that will acquire a dp1 state (Tozer et al., 2013). The temporal profile of BMP signalling target *Id2* confirmed that intracellular BMP signalling progressively decreased as soon as 1h after BMP4 addition (Samanta and Kessler, 2004; Hollnagel et al., 1999).

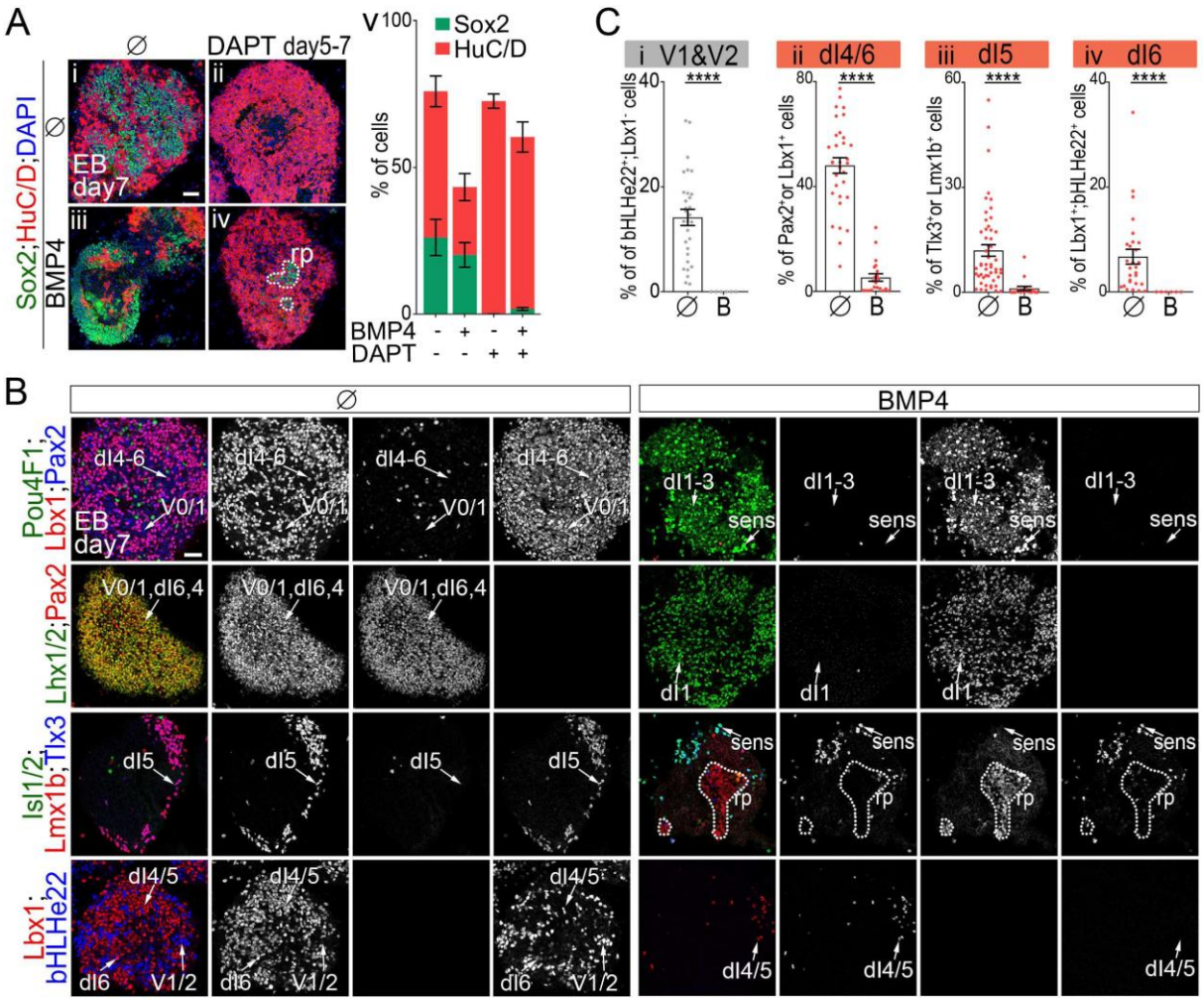

Fig. S3: Temporal and spatial dynamics in PM markers expression within dorsal spinal organoids

(A) Immuno-detection of Sox2 and HuC/D and DAPI labelling on day 7 EB cultured as in Fig. 1A treated with or without DAPT and with or without BMP4 (i-iv, scale bar: 60µM). Percentage of HuC/D$^+$ (red) and Sox2$^+$ (green) cells in day 7 mouse ESC derived EB grown in the indicated conditions (mean±s.e.m.). (v) BMP4 decreased the rate of differentiation of NP in EB. DAPT treatment from day 5 pushed BMP4 treated or not treated cells towards a terminally differentiated HuC/D$^+$ state.

(B) Immuno-detection of the indicated IN subtype markers on day 7 organoids treated or not with BMP4. Dash lines surround rp territory (scale bar: 60µM). **(C)** Percentage of ventral and associating IN subtypes harbouring the indicated TF code per image field (circles: individual values, bars: mean±s.e.m.). In absence of BMP4, the vast majority of cells within the organoid harboured a molecular identity reminiscent of one of the three major classes of early born associating neurons. It included 5% of Lbx1$^+$;bHLHe22$^+$ dI6 cells, 12% of Lbx1$^+$; Pou4f1$^+$ or Tlx3$^+$;Lmx1b$^+$ peripheral dI5 cells, and 45% of Lbx1$^+$;Pax2$^+$;bHLHe22$^-$ like cells. The remaining 20% of cells displayed a ventral V2 to V0 IN states. In presence of BMP4 these cell-types were no longer produced in the EB. Instead, a variety of dorsal cells were present in the organoids.

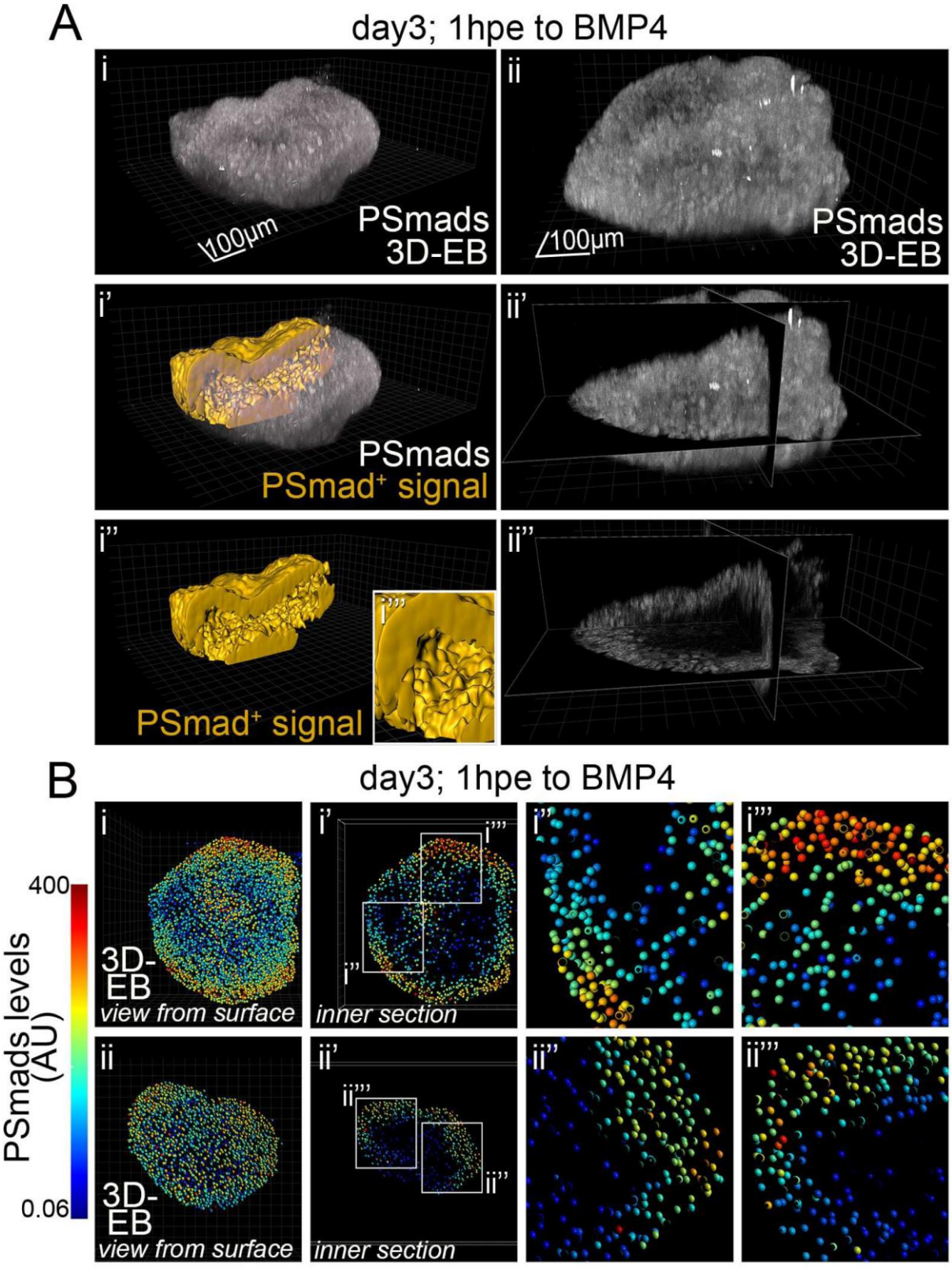

Fig. S4: Spatial restriction of BMP4 mediated Smads activation observed in whole EB

(A) (i,ii) 3D-Reconstruction of whole EB stained for PSmads. **(i'-i''')** Surfaces (in yellow) delimitating PSmads^{+} cells in an EB cut in half with optic scissors, with ii''' a blow-up showing that inner part of the EB is devoid of PSmad signal. **(ii'-ii'')** Position of 3 section plans throughout an EB and signal detected at the level of these plans. *These images demonstrate that Smads activation was restricted to the periphery of whole EB.* **(B)(i,ii)** View from the surface of all segmented cells of an EB. **(i',ii')** Inner optical sections through the EB showing cells displaying some PSmad signal. **(i'', ii'', i''', ii''')** Blow up on two distinct areas, showing in each case an outer-inner gradient of PSmad levels. Smads activation across the outer epithelium displayed a gradient, whose amplitude varied throughout this epithelium.

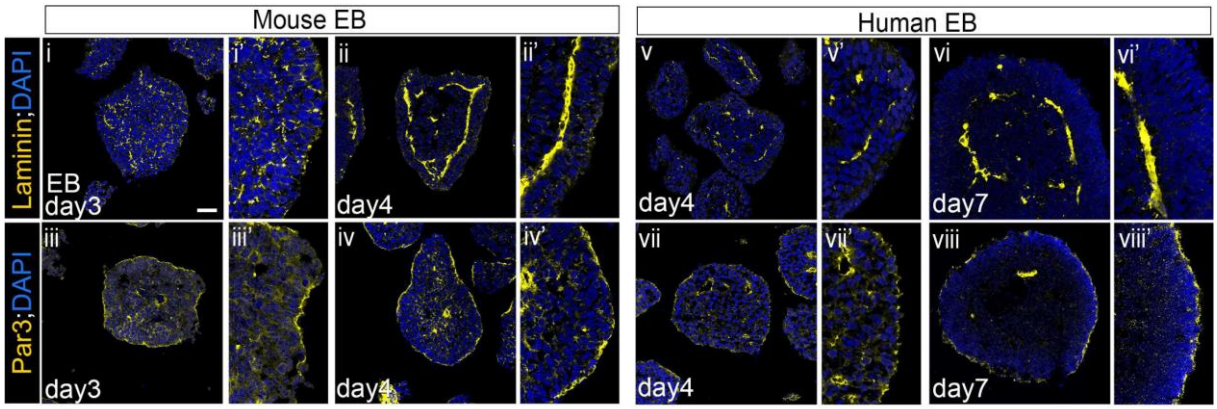

Fig. S5: Par3 and laminin distribution in mouse and human EB during the course of their differentiation

Laminin and Par3 immuno-detection and DAPI labelling in mouse and human EB at the indicated day of differentiation. x' panels are blown up of regions of the x panel (scale bar: 60µM).

Strong Par3 signal delineated the peripheries of the EB and of small lumen inside the EB at all the stages analysed both in human and mouse EB. Laminin was scattered within both mouse and human EB at an early stage of differentiation (day 3 in mouse and day 4 in human), yet it started accumulating and forming a ring separating an outer epithelium from inner epithelia. At later stages of differentiation (day 4 in mouse and day7 in human), this ring was well defined in both species.

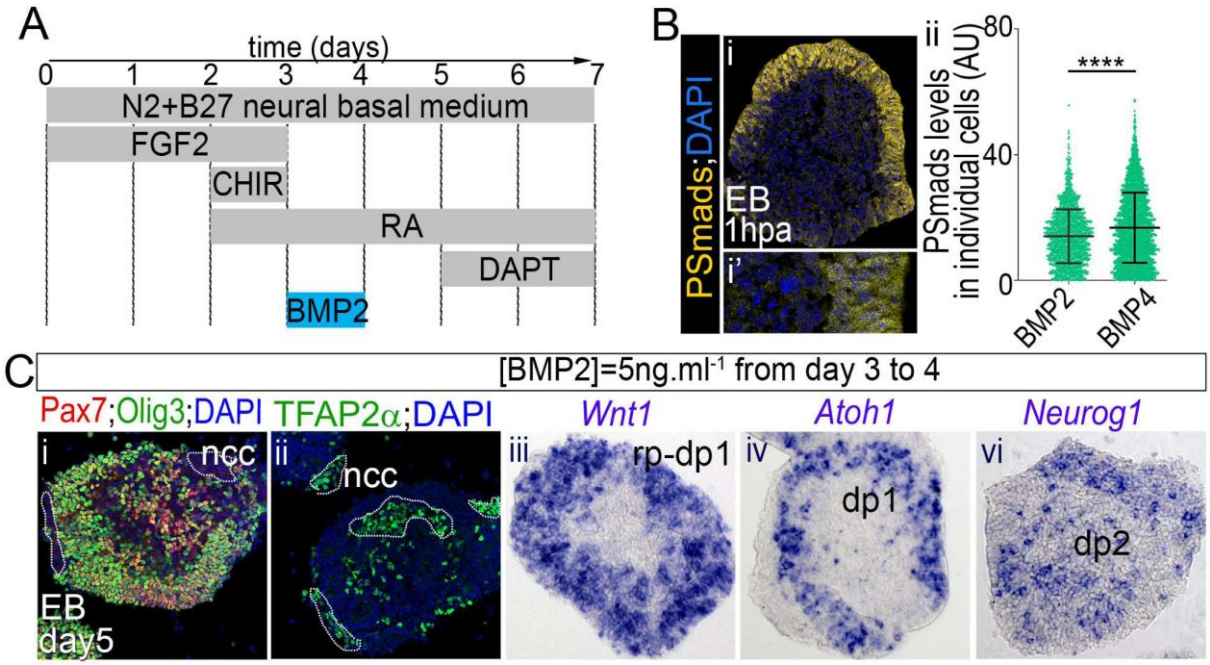

Fig. S6: BMP2 mediated pattern formation

(A) Schematics of the conditions used for the differentiation of the EB shown in Fig. S6. *Note that BMP2 was used instead for BMP4*. **(B)** Immuno-detection of phospho-Smad1/5/9 (PSmads) and DAPI labelling in EB grown 1hour after BMP2 addition to the medium (**i**) and graphs showing the differences between the levels of PSmads in EB cells cultured with BMP2 or BMP4 (**ii**) (mean±s.d., $p<0.0001$). **(C)** Immuno-detection (**i-ii**) and ISH (**iii-vi**) for the indicated NP markers. White dash lines surround ncc territory (scale bar= 60µM).

As observed for BMP4, BMP2 mediated Smads activation was restricted to the outer EB epithelium (Bi). Despite lower levels of Smads activation than measured in presence of BMP4 (Bii), patterns of BMP2 dependent-gene expression were generated in the EB (C), reminiscent to those observed in EB grown with BMP4 (Fig. 1).

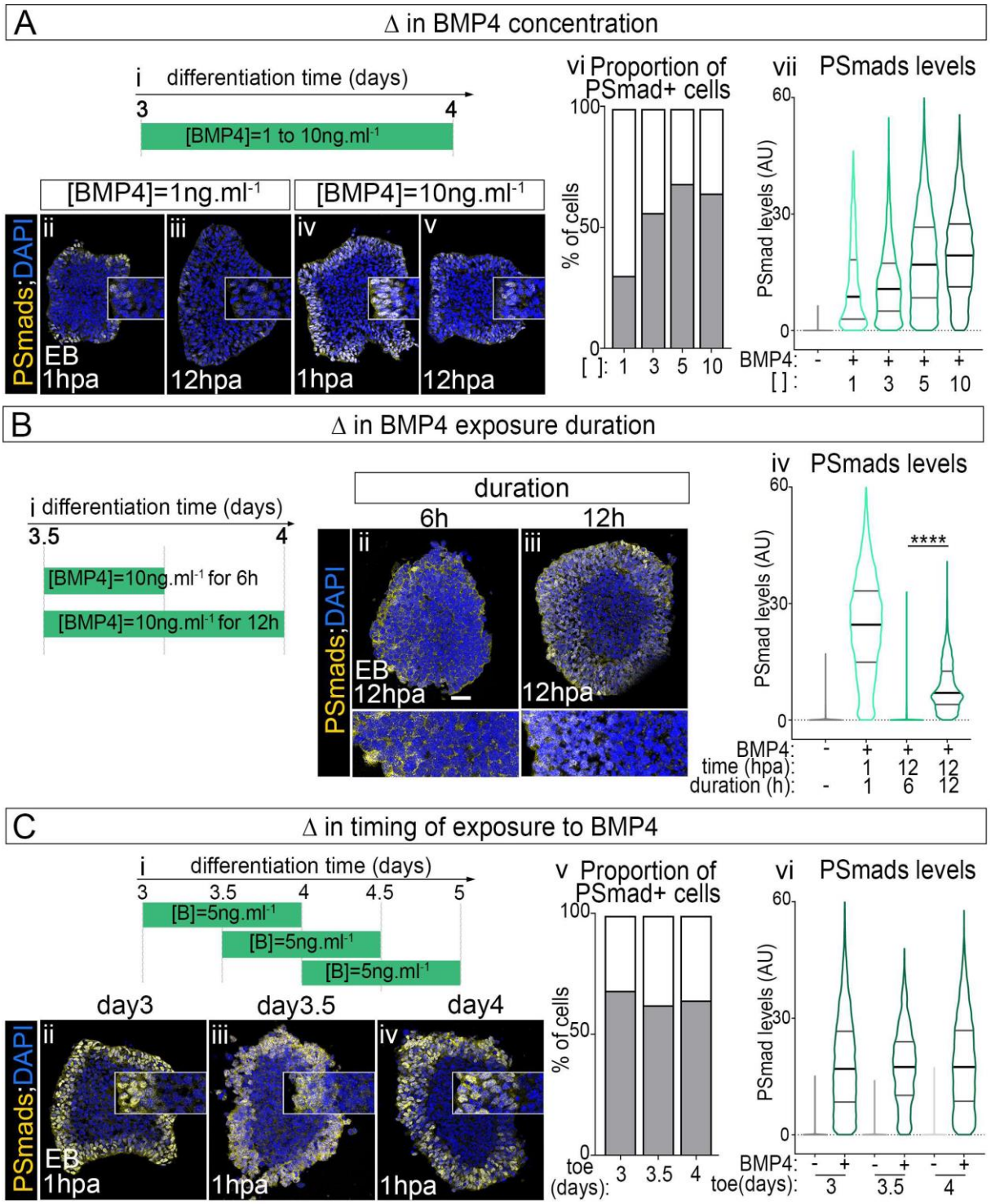

Fig. S7: Effects of BMP4 concentration, exposure duration and timing on Smads activity

Characterization of modulating BMP4 concentration **(A)**, exposure duration **(B)** and timing **(C)** on PSmads levels, spatial distribution and temporal dynamics. **(Ai, Bi, Ci)** Schematics showing BMP4 exposure time windows and concentrations used. **(Aii-v, Bii,iii, Cii-iv)** Immuno-detection of PSmads and DAPI labelling in EB at the indicated time points and conditions (hpa; hour post BMP4 addition). Insets in A and C and lower panels in B are blown ups on PSmads^{+} region. **(Avi, Cv)** Proportion of PSmads^{+} cells per image field. **(Avii, Biv, Cvi)** Violin plots showing PSmads levels in EB cells grown in the indicated conditions.

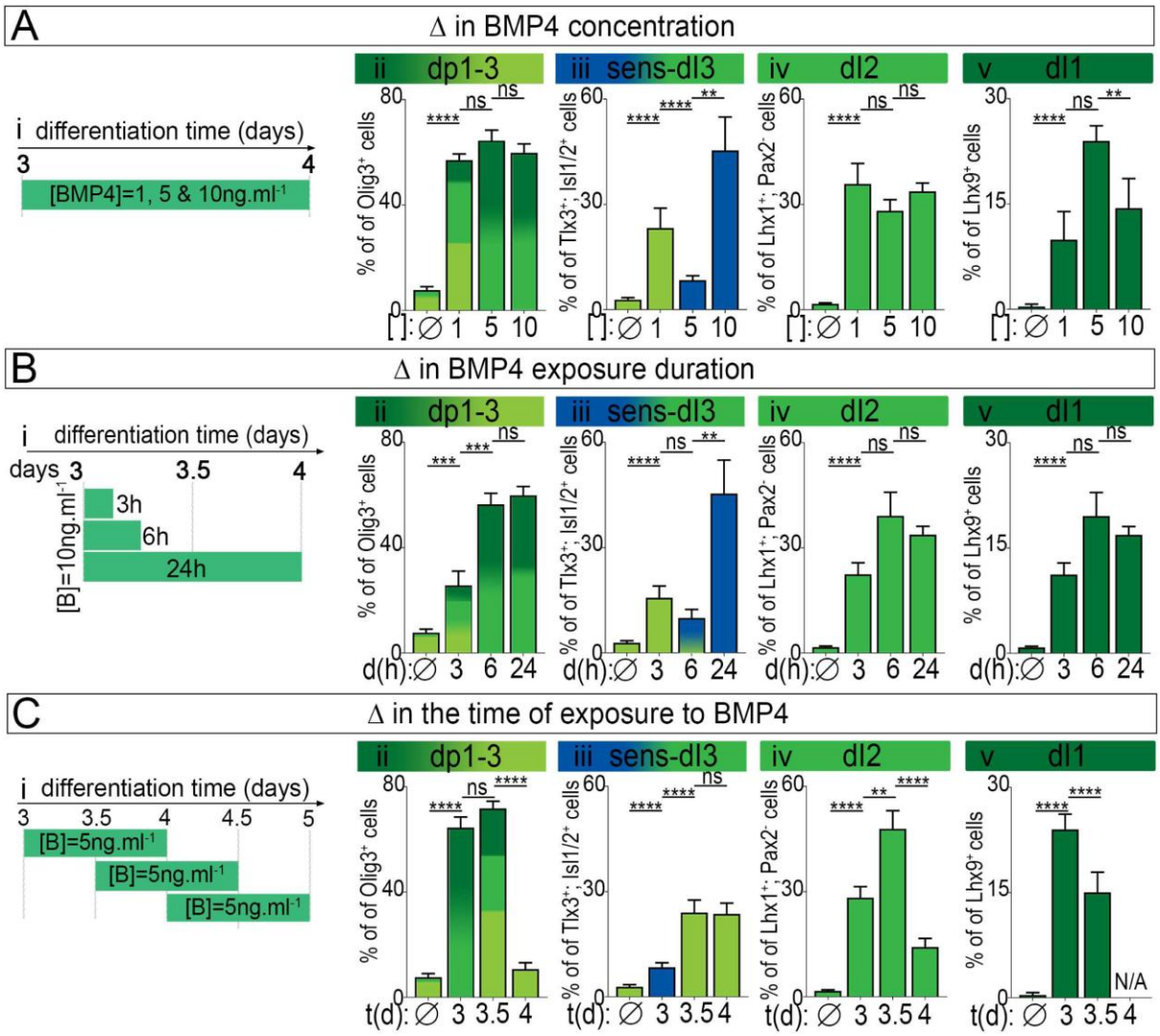

Fig. S8: Effects of BMP4 concentration, exposure timing and duration on the generation of relay IN

Quantifications of the percentage per image field of dp1-dp3 Olig3^{+} NP, dI3, dI2, dI1 and ncc derived sensory cells coloured-coded as in Fig. 1A (circles: individual values, bars: mean±s.e.m.) upon the modulation of BMP4 concentration **(A)**, BMP4 exposure duration **(B)** and the timing of exposure **(C)**. In (**i**), schematics showing the time period and the concentration of BMP4 used. Increasing BMP4 concentration, duration exposure and advancing the time, at which BMP4 was added, promoted the generation of cells with a more dorsal identity.

Table S1. Primer sequences used for qRT-PCR on mouse EB

Fw-*Atoh1*: GCTGGTAAGGAGAAGCGGCTGTG

Rev-*Atoh1*: TGTACCCCATTCACCTGTTTGC

Fw-*Fgf5:* TGTACTGCAGAGTGGGCATC (from (Turner et al., 2017))

Rev-*Fgf5:* ACAATCCCCTGAGACACAGC (from (Turner et al., 2017))

Fw-*Hoxb1:* GGTCAAGAGAAACCCACCTAAG

Rev-*Hoxb1:* CACGGCTCAGGTATTTGTTG

Fw-*Hoxb4*: CACGGTAAACCCCAATTACG

Rev-*Hoxb4*: GAAACTCCTTCTCCAACTCCAG

Fw-*Hoxc6*: ACACAGACCTCAATCGCTCAG

Rev-*Hoxc6*: CGAGTTAGGTAGCGGTTGAAG

Fw-*Id2*: CTCCAAGCTCAAGGAACTGG

Rev-*Id2*: TGCTATCATTCGACATAAGCTCAG

Fw-*Klf4:* GGAAGGGAGAAGACACTGCG

Rev-*Klf4:* ATGTGAGAGAGTTCCTCACGCC

Fw-*Neurog1*: GACACTGAGTCCTGGGGTTC

Rev-*Neurog1*: GTCGTGTGGAGCAGGTCTTT

Fw-*Neurog2*: GTGCAGCGCATCAAGAAGAC

Rev-*Neurog2*: TGAGCGCCCAGATGTAATTG

Fw-*Nkx1.2:* ACTGCCTTCACTTACGAGCA

Rev-*Nkx1.2:* AAATTTTGACCTGCGTCT

Fw-*Pou5f1:* AGTTGGCGTGGAGACTTTGC

Rev- *Pou5f1:* CAGGGCTTTCATGTCCTGG

Fw-*TBP*: GAAGAACAATCCAGACTAGCAGCA

Rev-*TBP*: CCTTATAGGGAACTTCACATCACAG

Table S2. List of antibodies

Antigen	Species	Dilution	Provider (reference)
bHLHE22	Rabbit	1/2500	Abcam (ab204791)
Brachuyry	Goat	1/300	R&D systems (AF2085)
Pou4f1	Mouse	1/400	Chemicon (A5945)
Cdx2	Rabbit	1/1000	Abcam (76541)
Dbx1	Rabbit	1/100	Pierani et al., 1999
FoxD3	Guinea pig	1/5000	From T. Müller and K. Birchmeier (Muller et al., 2005)
Gsx2	Rabbit	1/3000	Millipore (Gsh2, ABN162)
Hoxa5	Rabbit	1/1000	Sigma (HPA029319)
HuC/D	Mouse	1/1000	Thermo Fisher Scientific (16A11)
Islet1/2	Mouse	1/50	DHSB clone 39.4
Laminin	Rabbit	1/500	Sigma (L9393)
Lbx1	Guinea pig	1/10000	From T. Muller and K. Birchmeier
Lhx1/5	Mouse	1/20	DSHB (4F2)
Lhx9	Goat	1/200	Santa Cruz (sc19350 E-14)
Lmx1b	Rabbit	1/10000	From T. Muller and K. Birchmeier
Lmx1b	Guinea pig	1/10000	From T. Muller and K. Birchmeier
Nkx6.1	Mouse	1/50	DSHB (F55A10)
Olig3	Guinea pig	1/10000	From T. Muller and K. Birchmeier
Par3	Rabbit	1/1000	Millipore
Pax2	Rabbit	1/500	Thermo Fisher Scientific (716000)
Pax6	Rabbit	1/250	Biolegend (PRB-278P)
Pax6	Mouse	1/50	DHSB (AB 528427)
Pax7	Mouse	1/50	DSHB (PAX7)
PSmad1/5/9	Rabbit	1/250	Cell Signalling Technology (13820S)
Sox1	Goat	1/200	R&D systems (AF3369)
Sox2	Rabbit	1/200	Thermo Fisher Scientific (48-1400)
Sox9	Goat	1/100	R&D systems (AF3075)
TFAP2α	Rabbit	1/100	Santa Cruz (sc8975)
Tlx3	Rabbit	1/10000	From K. Birchmeier
Secondary antibodies: donkey against mouse, goat, guinea pig or rabbit IgG coupled to Alexa Fluorophores A488, A546, A568 or A647 (Thermo Fisher Scientific) were diluted 1:300 and used with DAPI (500ng/ml, Sigma, 28718-90-3).			

References

Andrews, M. G., del Castillo, L. M., Ochoa-bolton, E., Yamauchi, K., Smogorzewski, J., Butler, S. J., Castillo, L. M., Ochoa-bolton, E., Yamauchi, K., Smogorzewski, J., et al. (2017). BMPs direct sensory interneuron identity in the developing spinal cord using signal-specific not morphogenic activities. *Elife* **6**, 1–24.

Beccari, L., Moris, N., Girgin, M., Turner, D. A., Baillie-Johnson, P., Cossy, A.-C., Lutolf, M. P., Duboule, D. and Arias, A. M. (2018). Multi-axial self-organization properties of mouse embryonic stem cells into gastruloids. *Nature* **562**, 272–276.

Briscoe, J., Pierani, A., Jessell, T. M. and Ericson, J. (2000). A homeodomain protein code specifies progenitor cell identity and neuronal fate in the ventral neural tube. *Cell* **101**, 435–445.

Britz, O., Zhang, J., Grossmann, K. S., Dyck, J., Kim, J. C., Dymecki, S., Gosgnach, S. and Goulding, M. (2015). A genetically defined asymmetry underlies the inhibitory control of flexor–extensor locomotor movements. *Elife* **4**, 1–22.

Dasen, J. S., Tice, B. C., Brenner-Morton, S. and Jessell, T. M. (2005). A Hox regulatory network establishes motor neuron pool identity and target-muscle connectivity. *Cell* **123**, 477–91.

Henrique, D., Abranches, E., Verrier, L. and Storey, K. G. (2015). Neuromesodermal progenitors and the making of the spinal cord. *Development* **142**, 2864–2875.

Hollnagel, A., Oehlmann, V., Heymer, J., Rüther, U. and Nordheim, A. (1999). Id genes are direct targets of bone morphogenetic protein induction in embryonic stem cells. *J. Biol. Chem.* **274**, 19838–45.

Lee, K. J., Dietrich, P. and Jessell, T. M. (2000). Genetic ablation reveals that the roof plate is essential for dorsal interneuron specification. *Nature* **403**, 734–40.

Liu, J. P., Laufer, E. and Jessell, T. M. (2001). Assigning the positional identity of spinal motor neurons: rostrocaudal patterning of Hox-c expression by FGFs, Gdf11, and retinoids. *Neuron* **32**, 997–1012.

Moody, S. A. and LaMantia, A.-S. (2015). Transcriptional Regulation of Cranial Sensory Placode Development. *Curr Top Dev Biol.* **111**, 301–350.

Muller, T., Anlag, K., Wildner, H., Britsch, S., Treier, M., Birchmeier, C. and Müller, T. (2005). The bHLH factor Olig3 coordinates the specification of dorsal neurons in the spinal cord. *Genes Dev* **19**, 733–743.

Pierani, A., Brenner-Morton, S., Chiang, C. and Jessell, T. M. (1999). A Sonic hedgehog-independent, retinoid-activated pathway of neurogenesis in the ventral spinal cord. *Cell* **97**, 903–915.

Samanta, J. and Kessler, J. A. (2004). Interactions between ID and OLIG proteins mediate the inhibitory effects of BMP4 on oligodendroglial differentiation. *Development* **131**, 4131 LP-4142.

Sasai, N., Kutejova, E. and Briscoe, J. (2014). Integration of signals along orthogonal axes of the vertebrate neural tube controls progenitor competence and increases cell diversity. *PLoS Biol.* **12**, e1001907.

Tozer, S., Le Dréau, G., Marti, E., Briscoe, J. and Le Dreau, G. (2013). Temporal control of BMP signalling determines neuronal subtype identity in the dorsal neural tube. *Development* **140**, 1467–74.

Turner, D. A., Girgin, M., Alonso-Crisostomo, L., Trivedi, V., Baillie-Johnson, P., Glodowski, C. R., Hayward, P. C., Collignon, J., Gustavsen, C., Serup, P., et al. (2017). Anteroposterior polarity and elongation in the absence of extra-embryonic tissues and of spatially localised signalling in gastruloids: mammalian embryonic organoids. *Development* **144**,.

Zagorski, M., Tabata, Y., Brandenberg, N., Lutolf, M. P., Tkačik, G., Bollenbach, T., Briscoe, J. and Kicheva, A. (2017). Decoding of position in the developing neural tube from antiparallel morphogen gradients. *Science (80-.).* **356**, 1379–1383.